Highly efficient antimicrobial ceramics based on electrically charged interfaces

JULIAN JIMENEZ REINOSA, Miguel Muñoz Rojo, Adolfo Del Campo, Marisol S. Martin-Gonzalez, and Jose F. Fernandez

Just Accepted

Highly efficient antimicrobial ceramics based on electrically charged interfaces

Julián Jiménez Reinosa*[1], Miguel Muñoz Rojo[2], Adolfo del Campo[1], Marisol Martín-González[3], José Francisco Fernández[1]

1. Instituto de Cerámica y Vidrio (ICV-CSIC), C/ Kelsen 5, E-28049, Madrid. Spain.

2. University of Twente, Thermal and Fluid Engineering 5, Drienerlolaan, 7500 AE Enschede, Enschede, NL 7500 AE.

3. Instituto de Micro y Nanotecnología (CNM-CSIC), C/ Isaac Newton 8, PTM, E-28760, Tres Cantos. Spain

*Corresponding author: Julián Jiménez Reinosa.

E-mail: jjreinosa@icv.csic.es

Postal adress: Instituto de Cerámica y Vidrio, Consejo Superior de Investigaciones Científicas, C/ Kelsen 5, 28049, Madrid. Spain.

Telephone: + 34 91 735 58 40

ABSTRACT

The increasing threat of multidrug-resistant microorganisms is a cause for worldwide concern. This motivates a necessity to discover new antimicrobial agents or new mechanisms for microorganism eradication, different from those currently used. Here, we report an effective antibacterial ceramic glaze that combines different bactericide mechanisms. Specifically, the used methodology of the glaze results in glass-free edge crystallizations of feldspar structures at the ceramic surface. A combination of Rutherford Backscattering Spectroscopy (RBS), Scanning Electron Microscopy (SEM) and Raman Microscopy is used in order to determine the chemical elements and crystallizations at the ceramic surface. Moreover, Kelvin Probe Force Microscopy (KPFM) demonstrates that the presence of glass-free edges in feldspar needle crystals (semiconductor phase) on a glass matrix (insulator phase) promotes the formation of Semiconductor-Insulator Interface barriers. These barriers act as reservoirs of electric charge ~1.5V producing a discharge exceeding the microorganism membrane breakdown value (up to 0.5V). Furthermore, the surface crystallizations account for the formation of a micro-roughness that limits biofilm formation. Both factors result in high antibacterial activity in the range of R > 4 for *Escherichia coli* and *Staphylococcus aureus*. This approach opens new possibilities to attain bactericidal surfaces and to understand the role of physical interaction as a main antimicrobial mechanism.

KEYWORDS

Ceramic tile; antimicrobial properties; feldspar crystallizations; surface charge; physical mechanisms.

1

1.- Introduction

One of Today's challenge is providing reliable long-term antibacterial protection to objects used by humans. The ability of bacteria and other microorganisms to resist the effects of an antibiotic to which they were once sensitive is one of the most important social and materials-engineering problems. The increase in epidemics with different aetiology and in constant modification is evolving faster due to the overuse of antibiotic substances. The situation claims thousands of human lives every year and results in the decrease of the effectiveness of existing solutions in fighting the multiplication of pathogenic bacteria. As a consequence, a great deal of attention is being focused on developing and using antibacterial solutions in industrial, public and domestic areas.[1]

The antibacterial effect is demanded in a quite large variety of products and applications such as textile, household cleaning, home appliances, furniture, transport vehicles, cosmetic products, sanitary ware, tableware, coverings, etc. Among them, the demand for bactericidal solutions related to ceramic tiles is of great interest due to their durability and easy cleanability. Typically, ceramics are present in rooms with high humidity conditions, like bathrooms or kitchens, where resistant microorganisms are able to infect humans. The most common bacteria in wet areas of domestic environments are *Staphylococcus aureus*[2] and *Escherichia coli.*[3] These are usually found in floors and walls, surfaces which are normally covered by ceramic tiles with glazed surfaces. The ceramic surface is easy to clean and to disinfect but does not possess an intrinsically antibacterial effect. Tiles require junctions between units that are more difficult to disinfect and for such reason, mortars for tiles junctions with antibacterial properties were developed.[4]

In order to produce a ceramic surface with antibacterial properties, different solutions have been developed. The ceramic tile having a glaze with antibacterial properties is described on the base of different mechanisms based on physical mechanisms, chemical mechanisms or a combination of both. In the case of physical mechanisms that promote chemical reactions, a family of bactericide glazes needed to be activated by UV photons nearest to the visible region of the spectrum.[5] In this case, the photoactivity of materials such as TiO_2 or CeO_2 generates exciton pairs which generate free radicals (e.g. hydroxyl radicals) that are able to undergo secondary reactions. The electronic transfers may be capable of causing redox processes on biological matter, such as bacteria deposited on or in close contact with glazed surfaces.[6] Nevertheless, these ceramic surfaces are not useful indoors as they require UV light irradiation.

Another chemical mechanism, apart from redox reactions by free radicals, was also explored in glazed surfaces. The lixiviation of cations from glass structure, as Ca^{2+}, provokes biocide activity due to depolarization of the cell membrane as a consequence of the very high punctual concentration of Ca^{2+} at the bacteria membrane.[7] Among chemical lixiviation of species, some materials as metallic silver,[8] silver salts[9] or copper oxide nanoparticles[10] at the glaze surface are toxic for microorganisms. However, the main limitation of species lixiviation is their durability,

2

decreasing the antibacterial effect over time. Additionally, copper or silver cations lead to the formation of dark colors in the ceramics, which limits their use.

It is reported the presence of large amounts of bacteria in ceramic floor tiles, and therefore the high possibility of their migration towards food.[11] The surface roughness of tiles has a direct relation with the cleanability of that surface, and thus the presence of bacteria.[12] These are primarily present in kitchens and bathrooms in domestic environments, but also in urban environments, in which cleanability is of higher importance. It is described that specific roughness grants glass surface bacteria-repellent properties[13] as it inhibits bacterial adhesion. In this sense, there is a growing interest to design antibacterial and antifouling surfaces based on micro-roughness engineering that inhibited biofilm formation.[14] Moreover, recent studies on ZnO microparticles point out the existence of semiconductor interfaces able to cause damage to the cellular wall by local electric charge transfer.[15]

The transfer of organism around the World and the development of new microorganisms along with the climate change that is possibly taking place, cause the need to protect ourselves against such pathogenic species. The application of scientific studies has given raise antibacterial ceramics and tiles to be used in hospitals, centers for childhood, schools, spas, public toilets, etc. But the functionality of the actual ceramics is limited in time (in the case of lixiviation of antibacterial ions) or requires unusual treatments at the place of antimicrobial action (as UV irradiation). In addition, despite the high number of studies that take into account different antimicrobial mechanisms, there is still a gap in the understanding of the effective mechanisms behind bacterial death. In this work, we propose a newly designed ceramic glaze having feldspar crystallizations with glass-free edges at the surface. In addition to the microroughness, the surface exhibits highly antibacterial properties due to the electrical charge originated between the feldspar microcrystals and the insulating glass. In this sense, the proposed solution overcomes the durability limits of the previous antibacterial mechanism used for ceramic tiles and with an antibacterial effect with increased durability.

2.- Experimental procedure

Two different compositions were used to obtain the antibacterial ceramic glaze (table 1). Materials corresponding to industrial standards are used in stoneware industry and were supplied by Kerafrit S.A. The differences in composition give rise to glazes with distinct viscosity behaviour with temperature denoted as A and B glazes. The glazes were prepared following a standard procedure in the ceramic tile industry.[16] Hence, homogeneous suspension in water of commercial frit and Kaolin was prepared. The solid content was 40 wt % and the relative mass proportion of each component on the solid was: 90 wt % frit, 10 wt % Kaolin. The suspension was homogenized by ball milling for a period of 20 min using 0.2 wt % of sodium tripolyphosphate as deflocculant and 0.2 wt % of carboxymethyl cellulose to improve the adhesion of the glaze to the green tile. The suspension was sprayed on the surface of a

stoneware green tile substrate producing coatings with thicknesses of ca.250 μm - ca. 200 μm of glaze B deposited over the stoneware green tile and ca. 50 μm of glaze A deposited over glaze B (see supplementary information figure S1). Following deposition, the tiles were dried at 90 °C and fast-fired in an air atmosphere using a Pirometrol furnace. The heating rate was ca. 30 °C/min and the maximum temperature was 1200 °C (held for 5 min). This sintering cycle corresponds to a standard industrial fast-firing process of stoneware ceramic tiles. The total duration of the firing cycle was 55 min.

Table 1.- Chemical compositions of glazes A and B which were formulated for this work.

Frit composition (wt %)	Na_2O	K_2O	CaO	MgO	ZnO	Al_2O_3	B_2O_3	SiO_2	Total
Glaze A	4.97	2.88	7.98	2.75	7.72	20.29	0.47	51.54	98.60
Glaze B	5.13	3.12	8.84	3.12	0.42	22.33	0.50	55.28	98.74

Hot-stage microscopy of the glaze compositions was carried out in the range 30–1220 °C with a heating rate of 10 °C/min by a Leica Leitz microscope. The glaze surfaces were characterized by X-ray diffraction analysis, performed with Cu Kα radiation using a Siemens D500 Diffractometer in grazing angle (0.5°2θ) the step time being 2 s with an increase of 0.02°2θ. The glazes were also characterized by Rutherford backscattering spectrometry (RBS) to assess the in-depth distribution of the elements from the surface of the glass layers. As far as we are aware, RBS is the only nondestructive technique able to provide precisely the thickness and composition of coating thin layers,[17,18] by measuring the energy distribution of the elastically backscattered particles. RBS was performed at the microbeam line (Centre for Micro Analysis of Materials, University Autonoma of Madrid), using a beam of α particles ($4He^{2+}$) with a beam size of approximately 1.5 mm. To significantly improve the accuracy of the elemental surface concentration values, the energy of the beam was set according to the atom of the element to be determined: 2.0 MeV for heavy elements such as zinc and silica and 3.035 MeV for oxygen. At the later energy, the 16O(α,α)16O non-Rutherford elastic backscattering resonance occurs and the sensitivity to detect oxygen is increased by a factor of 23.[19] The obtained spectra were interpreted with the simulation code SIMNRA.[20]

A lixiviation assay of glazes was performed by incorporating $1cm^2$ of sintered glaze into 100mL of de-ionized water during 24 hours under stirring while keeping the temperature at 30ºC. The chemical analysis of Zn^{2+}, Ca^{2+} and Na^+ into the water after the lixiviation assay was determined in an Inductively Coupled Plasma Optical Emission Spectroscopy (ICP-OES) analysis by using an Iris Advantage Spectrometer from Termo Jarrel Ash. The Raman study with the use of a confocal Raman coupled with an AFM was carried out (Witec alpha300R, Witec, Ulm, Germany). Raman spectra were obtained using a 532 nm excitation laser (green laser). Raman

4

spectral resolution of the system is ca. 0.02 cm^{-1}. The microscopy setup is mounted in a piezo-driven scan platform having 4 nm lateral and 0.5 nm vertical positioning accuracy. The piezoelectric scanning table allows three-dimensional movement in steps of 3 nm, giving a very high spatial resolution for the Confocal Raman microscopy. The microscope base was also equipped with an active vibration isolation system, active 0.7–1000 Hz. Collected spectra were analysed by using Witec Control Plus Software (Witec, Ulm, Germany). The microstructure of the chemical etched (10% v/v HF/H2O) and gold coated glazes were also investigated by using a Field emission scanning electron microscope, FE-SEM, Hitachi S-4700.

Kelvin Probe Force Microscopy (KPFM) assay was developed to determine the local surface potential SP at sub-micrometre-scale, in this case, the contact potential difference V CPD between tip and sample, by measuring the electrostatic tip-sample interaction. Here, KPFM measurements were performed using a two-pass technique. During the first pass, a profile of the surface topography is acquired. The surface potential is then recorded in a second pass. During the second pass, the AFM tip follows the topography profile of the first pass at a pre-defined lift height of a few nanometers to some tens of nanometers. During the second pass, the cantilever is only electrically excited by applying an AC voltage (V AC sin (xt)) and a DC offset voltage V DC. The first harmonic force Fx causes cantilever oscillations at a frequency x of the AC voltage. Fx is proportional to the difference between the local tip-surface SP difference and the DC offset voltage (V CPD – V DC). By adjusting V DC to match V CPD, the first harmonic force vanishes and the cantilever oscillations at frequency x are nullified. The corresponding V DC values are monitored as a function of the lateral position, resulting in a two-dimensional map of the V CPD distribution.

The bactericide characteristics of the coatings were measured according to the standard JIS Z 2801. Control and test surfaces are inoculated with 10^5 colony-forming units (CFU) of microorganisms and they are allowed to incubate undisturbed in a humid environment for 24 h. After incubation, microbial concentrations are determined. Reduction of microorganisms relative to initial concentrations and the control surface is calculated according to the parameter R, bactericide effect is considered when R>2, accordingly with the following expression:

R = log (CFU $_{on\ control\ sample}$ / CFU $_{on\ test\ sample}$)

3.- Results and discussion

3.1 Antimicrobial activity of glazes.

The obtained glaze containing a combination of glaze A and glaze B show a glossy surface and, to the naked eye, it is free of defects, similar to a standard glaze form ceramic industry. The bactericide response of combined A+B glaze, table 2, indicates its high effectiveness as antimicrobial, specifically for *Staphylococcus* and *Escherichia coli* of 99.99%, that is R≥4, with

respect to the reference A or B glaze. This R-value is also higher than the R-values previously reported in the literature for glazes.[21-26] In fact, glaze A and glaze B could not be considered as antimicrobial as they show R<2, which is not considered to have antimicrobial effects according to JIS Z 2801. It is worth mentioning that the main difference between glaze A and B is related to the ZnO content. As the presence of Zn^{2+} could damage bacteria membrane, their abundance in the glaze is a source of cations able to produce the antibacterial effect. A complementary study on the variation of the Ca^{2+} composition in glaze A and the Zn^{2+} composition in glaze B demonstrated that the presence of such chemical species does not provide an adequate antimicrobial response (see Supplementary information figure S2 that shows the comparison of the R values for the bacteria mortality). Additionally, the studied glass matrix of the glazes corresponds to a stable structure under chemical attack, so the cations involved in the lixiviated glass are in low amount. Nevertheless, the deposition of glaze A over glaze B promotes the effective antibacterial properties as the R-values confirm. This fact indicates that an extrinsic factor appears after the combined deposition of both glazes, which gives it the antibacterial characteristics. From here, glazes A, B and their combination (glaze A + glaze B) will be studied in order to determine the origin of such extrinsic factors. In this case, the antibacterial properties are shown for both Gram-positive (*Staphylococcus aureus*) and Gram-negative (*Escherichia coli*).

Table 2.- Antimicrobial activity of glaze A, glaze B and the combined glaze A+B deposited in layers. The antimicrobial effect is attained according to Standard JIS Z 2801 when R-value is higher than 2.

	Control sample		Glaze A			Glaze B			Glaze A + Glaze B		
	CFU_o	CFU	CFU_o	CFU	**R**	CFU_o	CFU	**R**	CFU_o	CFU	**R**
E. coli	$1.0 \cdot 10^5$	$7.2 \cdot 10^6$	$1.0 \cdot 10^5$	$1.4 \cdot 10^6$	**0.71**	$1.0 \cdot 10^5$	$0.6 \cdot 10^6$	**1.08**	$1.0 \cdot 10^5$	$8.5 \cdot 10^1$	**4.92**
S. aureus	$1.0 \cdot 10^5$	$1.2 \cdot 10^6$	$1.0 \cdot 10^5$	$7.6 \cdot 10^4$	**1.20**	$1.0 \cdot 10^5$	$2.1 \cdot 10^5$	**0.76**	$1.0 \cdot 10^5$	$0.7 \cdot 10^2$	**4.23**

3.2 Structural evolution of glazes with thermal treatment.

The formation mechanism of the bactericide surface is based on the existence of two glaze compositions with different viscosity at high temperature and different crystallizations. The heating microscopy results of the A and B glazes are shown in figure 2a, to follow their evolution as the temperature increases. As expected, the shrinkage behaves in concordance with the chemical composition of their corresponding frits (table 1). The initial softening of glass, at ca. 785ºC for Glaze A and at ca. 885ºC for glaze B is attributed to the kaolin presence. It is worth to remark that the presence of ZnO reduces the temperature and enlarges the shrinkage in this first reaction. Zn^{2+} is as a glass network disruptor that promotes smooth surfaces and reduction of melting temperatures.[27] The indicated contraction temperature is in concordance to the results in bibliography regarding frits with similar composition.[28] The main shrinkage started at ca.1045ºC for glaze A and at ca. 1075ºC for glaze B. The main shrinkage corresponds to the

melting of the glaze. At higher temperatures, an interruption of the melting occurs, 1130ºC for glaze A and 1160ºC for glaze B, due to a crystallization process of the glaze.

The differences between glaze A and B in the temperatures where softening, melting and crystallization occur are used to deposit a 50 μm layer of glaze A onto the 200 μm layer of glaze B (see supplementary information figure S1). Due to the chosen design, it is expected that glaze A diffuses through the glaze B region. XRD studies in figure 2b indicate that the crystallization presented in the glazes correspond to plagioclase type feldspar.[29] In addition, Gahnite ($ZnAl_2O_4$) crystallizations can be observed in glaze A which is favoured by the existence of ZnO in the composition. Nevertheless, in the combined glaze (glaze A + glaze B) only feldspar crystallizations are identified by XRD characterization. This means that Gahnite crystallizations are not present in the glaze and Zn^{2+} cations probably diffuse toward the glaze B region.
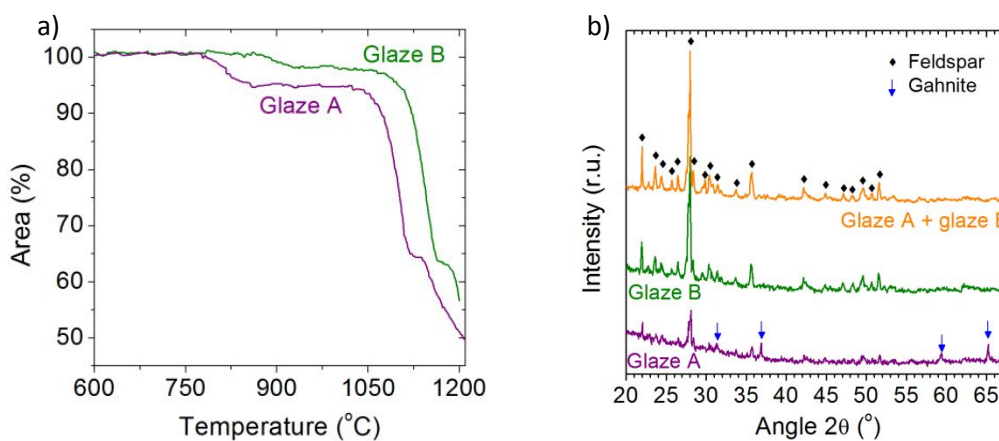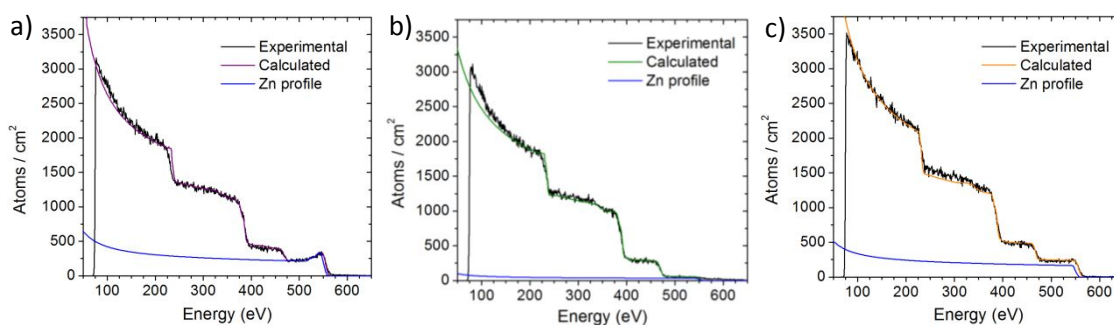

Figure 1.- a) Hot stage microscopy of A and B glaze compositions. b) XRD study of glazes A and B and their combination after sintering at 1200 °C. Glazes show plagioclase feldspars (JCPDS 01-084-0750) and moreover glaze A presents also Gahnite (JCPDS 00-005-0669).

The presence of cations in the medium of the bacteria could affect them by different mechanisms related with the bacterial cell wall as turgor or plasmolysis, due to the movement of charges for depolarization of the cell membrane after the fixation of cations.[30] Taking into account that the possibility of lixiviation of cations from the different glazes exists, a lixiviation assay into de-ionized water was carried out (table 3) and the concentration of the elements was obtained by ICP-OES. The glazes show a higher concentration of Zn^{2+}, Ca^{2+} and Na^+ than the de-ionized water, so partially the lixiviation of the studied cations takes place. Nevertheless, the concentration of lixiviate cations is low enough to affect the antibacterial behaviour because glaze A and glaze B do not present antibacterial properties. For instance, glaze A lixiviated the highest amounts of Zn^{2+} and Na^+ without relevant antibacterial effect. Moreover, the lixiviated Ca^{2+} amount for glaze B is similar than the amount lixiviated in combined graze A+B. In this sense, the cations lixiviation does not seem to be the responsible mechanism for the antibacterial characteristic in the studied glazes.

Table 3.- Ion concentration in water after the lixiviation assay of the glazes

| Ion concentration (μg/L)	[Zn^{2+}]	[Ca^{2+}]	[Na^+]
De-ionized water	24.3	135.1	26.8
Glaze A	87.1	154.1	213.5
Glaze B	26.4	405.8	201.2
Combined Glaze A + B	62.0	416.9	192.5

In order to know the distribution of both glazes compositions A and B after the sintering step, a RBS study was performed. In particular, the amount of zinc is taken into account since this chemical species differs between glazes composition. The technique is based on the inelastic collision between ions (α-particles in this case) and the atoms that make up the material. To find out the nature, concentration and distance to the surface of the elements, the energy of the dispersed ions (α-particles) is analyzed. Some cations (alkali and alkaline earth) present ease of movement in glass during the sintering process. Since RBS study allows knowing the disposition of the different atoms along a section of the studied sample and since glaze A and glaze B present different Zn amount, we studied the disposition of Zn in the combined glaze layer A+B from the initial glazes A and B. Hence, glaze A (figure 2a) and glaze B (figure 2b) profiles are compared with the combined glaze A+B (figure 2c). The chemical species are indicated depending on the maximum energy of the inelastic shock according to its mass. Glaze B presents an enrichment of zinc ions at the glaze layer which is not present in glaze A. Nevertheless, when the combined glaze A+B is analyzed, the average distribution of zinc atoms is observed. This means that Zn atoms are distributed along with the whole glaze layer in the combined glaze A+B. In addition, the absence of Gahnite crystallizations in the combined glaze A+B reinforces the evidence that the Zn-cations presence is homogenous along the glassy network of the glaze as a network disruptor. Hence, the designed layer of combined glaze A+B is based on the lower melting temperature of glaze that produces compositional homogeneity during the thermal treatment. As it was stated before, the chemical composition of the resulted glaze is not enough to provide the bactericide effect by itself. Regarding the rest of the chemical species into the glaze, like Na, K, Ca, Al or Si, RBS shows a homogeneous distribution along with the whole glaze layer as well (see supplementary information figure S3).

Figure 2.- RBS study of a) glaze A; b) glaze B; c) combined glaze A+B). Zn profiles (blue lines) are shown in order to determine the distribution of this element in the whole samples.

3.3. Microstructural analysis of glazes and correlation with their structural insights.

A Microstructural study of glaze A (Figure 3a) and combined glaze A+B (Figures 3b and 3c) was performed in order to confirm the existence of feldspar crystallizations. The as-sintered glaze surface presents a rough glassy surface showing characteristic feldspar crystallization in a glass matrix. At the surface of glaze A, the glassy phase is more generalized than in the combined glaze A+B that presents defined platelets shaped crystallizations with t particle size up to 15µm in length. Nevertheless, in glaze B these crystallizations are intuited in the interior of the glaze. The elongated morphology of the platelets shape grains supports their correspondence with feldspar crystallizations. In addition, the transversal microstructural study of the combined glaze A+B confirms the presence of platelets shaped grains that reach the surface of the glaze (Figure 3d). The platelet shape crystallizations are presented on the whole glaze thickness in different size and agglomeration state (see Supplementary information figure S4). The existence of crystallizations that protrude from the glaze surface may be relevant to the antibacterial mechanism since a high number of edges or angles at the glaze surface could erode the bacteria membrane. However, to perform the microstructural analysis of the transversal view of the glaze a chemical etching is required. As it is not guaranteed that the chemical etching is exclusively limited to the transversal cut, further analysis is required to elucidate the presence of shaped edges at the surface of the bactericide glaze.
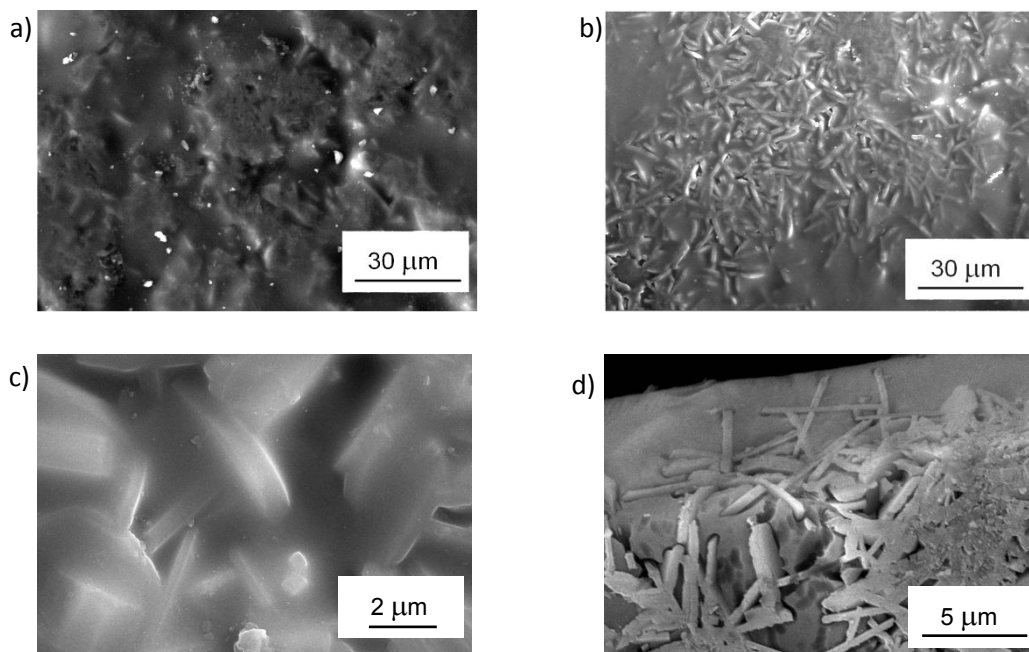
Figure 3.- SEM micrographs of a) Surface of Glaze B. b and c) Surface of combined glaze A+B. d) Transversal view of combined glaze A+B showing the existence of needle shape crystallizations at the glaze surface.

A study of the surface of the combined glaze A+B was performed by Confocal Raman Spectroscopy coupled with Atomic Force Microscopy. A study by Raman Spectroscopy allows the determination of the nature of the mentioned crystallizations observed by optical microscopy at the glaze surface. Therefore, the selected area in the optical micrograph (Figure 4a) was analyzed by AFM (figure 4b and 4f) and Raman Confocal Spectroscopy (figure 4c-4e). The AFM analysis revealed topography differences ranged up to 1250 nm in the selected area. Moreover, in the region where the crystallizations are more abundant, the roughness reached differences between peaks and valleys up to 200 nm. Two main Raman spectra are detected in the mentioned area: one that corresponds to the glassy phase and another one that corresponds to feldspars crystallizations (Figure 4c). These spectra are in agreement with the XRD study.

An initial comparison reveals that the main Raman spectra of the feldspars and glassy phase exhibit strong similarities in terms of the Raman shifts and relative intensities of major features. The glassy phase possesses broad Raman peaks at the Raman shift range of 800-1200 cm^{-1} and is similar to that of SiO_4 structural units, as the ones present in quartz structure, but with much weaker and broader signals.[31] The low structural order presented by the glass introduces a large variation of the bonding distances that is translated into Raman signal broadening. Also, in the glass Raman spectrum, polymerization of the structural units produces a broadening of the Raman bands at the Raman shift range of 800-1200 cm^{-1}.[32]

In the case of feldspar Raman spectrum, the defined Raman modes can be associated with Plagioclase (a mixture of Albite and Anorthite).[29, 33] The Raman modes at Raman shift 200-400cm^{-1} (signalled as A group) are assigned to deformations of the lattice as O-T-O and T-O-T, being T indistinctly Si or Al. The group of Raman bands C is related to the vibration of oxygen atoms movement along a line bisecting T-O-T bonds. In the case of F and G Raman bands groups, they correspond to Al-O-Si and Si-O-Si antisymmetric vibrations, respectively.[34] The Raman modes indicated as B, D and E are associated with feldspars which are rich in Calcium.[35] The position of the crystalline phases can be determined by Raman Spectroscopy from the Raman Spectrum of each measured position in the scanned area resulting in a Raman image of the surface of the glaze (Figure 4d). This technique shows the presence of crystallizations at the glaze surface for the combined glaze A+B. In addition, a depth Raman image of the surface (Figure 4e) reveals the presence of feldspar crystallization from the very top of the glaze surface. Such crystallization is uncovered by the glassy matrix and protrudes from the graze surface accordingly with the AFM analysis. A similar analysis on the surface of glaze A confirms that standard glaze composition possesses a continuous layer of glassy phase covering the surface crystallizations (see Supporting Information Figure S5). Whereas in the

standard glaze the crystallizations stay in the interior as it was previously inferred by SEM characterization, the designed glaze as a combined glaze A+B shows crystallizations that protrude from the glassy phase. This fact is generated by the lower melting temperature of the glaze A against glaze B that provokes the glassy phase diffusion of glass towards the bottom glaze layer. As a result, the crystallization exposed to the surface of the glaze in the designed glaze A+B. To sum up, the differences between the designed glaze as combined glaze A+B and a standard glaze (as A glaze) is the presence of protrude crystallizations at the surface. As the differences in chemical composition are not providing antibacterial characteristic, the determined microstructural differences of the surface must be on the origin of their high antibacterial efficiency for the combined glaze A+B.
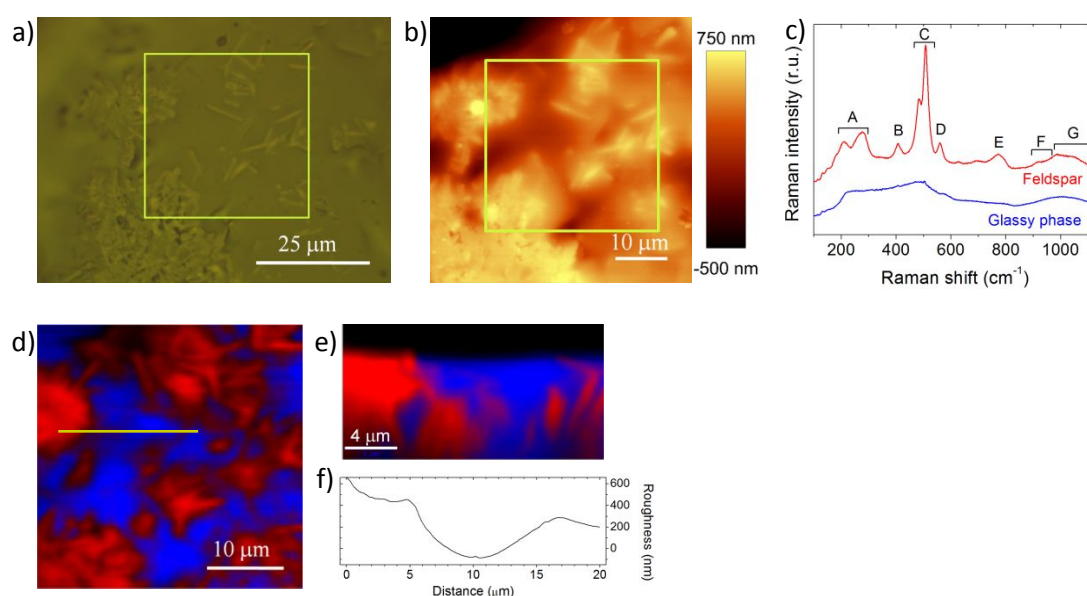

Figure 4.- Confocal Raman Microscopy coupled with Atomic Force Microscopy study of glaze A+B a) Optical microscopy of the glaze surface where the square denoted the area for AFM and by Confocal Raman Microscopy is performed; b) AFM (phase component) of the glaze surface and the studied area; c) Main Raman spectra of the phases determined in the square area glassy phase (signalled in red color) and plagioclase feldspar (signalled in blue color); d) Raman image of the glaze surface area showing the main Raman spectra distribution by color codes; e) Raman study as depth profile of glaze A+B showing the existence of feldspar crystallizations surrounded by glassy phase in the interior protruding from the surface of the glaze. f) Roughness profile from AFM study of the surface corresponding to the depth profile.

3.4 Functional characterization of the glaze surface and its correlation with the bactericide effect.

The existence of charge accumulation at the glass-free edges of the feldspar particles that protrude from the glassy phase is confirmed by Kelvin Probe Force Microscopy, Figure 5. In concrete, the work function is an extremely sensitive indicator of surface condition and is affected by adsorbed or evaporated layers, surface reconstruction, surface charging or oxide layer imperfections, among others. The outer surface potential has already been widely used to describe bacterial cell attachment to solid surfaces.[36] For this reason, Kelvin Probe Force Microscopy studies at different parts of the surface of the combined glaze A+B show that glassy phase does not present potential changes, nevertheless, surface areas of glaze with feldspar crystallizations (detected by topography signal, Figure 5b) show an increase of the potential values (Figure 5c). This fact means that an enlargement of charge exists where the crystallizations are present. Moreover, feldspar crystallizations protrude from the glass up to 200nm and are associated with potential exceeding 1.5 volts.
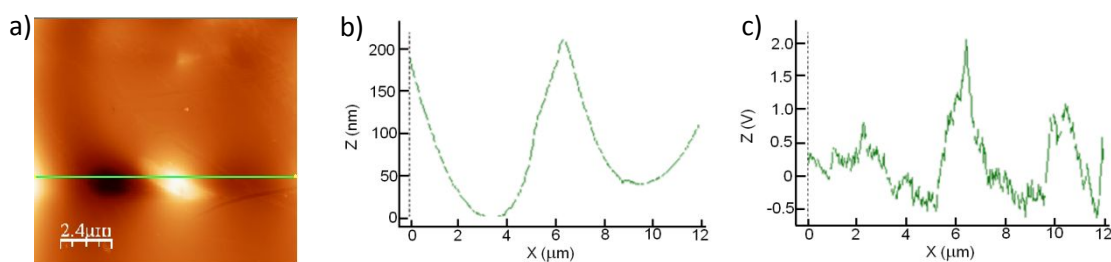

Figure 5.- KPFM of the glaze A+ B surface. a) AFM (phase contribution) image with the line across the protrude region associated with a feldspar crystallization. b) The topography of the glaze surface across a feldspar crystallization c) Surface potential across feldspar crystallization where charge accumulation occurs.

Regarding the presence of electrical charges in feldspar crystallizations, feldspars are crystalline aluminosilicates whose composition can be represented in terms of a ternary system: orthoclase ($KAlSi_3O_8$), albite ($NaAlSi_3O_8$) and anorthite ($CaAl_2Si_2O_8$). Feldspar crystallizes in monoclinic or triclinic systems and as XRD study showed for the studied glaze, triclinic structure governs. It consists of interlinked tetrahedrons of SiO_4 and AlO_4 which form a negatively charged 3D framework, and large cations such as K, Na or Ca, which occupy the interstices of the framework.[37] The presence of defects in the structure is usually due to the presence of chemical substitutions and to the high number of edges that micrometric platelet shape crystallizations present. Hence, charges are accumulated in the feldspar system. In addition, in the glaze, the existence of semiconductor particles of feldspar in an insulator matrix (glassy phase) would lead to the generation of semiconductor-insulation charge barriers, which is shown by KPFM. So, the existence on the one hand of edges and defects in feldspar structure and on the other hand of differences in conductivity between feldspar and glassy phase

facilitates the electric charge accumulation throughout feldspar as shown in the electric potential. In addition, the surface potential peaks determined by KPFM indicate local positive charge accumulation. The KPFM scanning used a dc-biased tip that results in the injection of free charge carriers. In addition, the presence of semiconductor particles of feldspar resulted in a discontinuity of polarization in the insulator glass matrix. The KPFM charge presents a peak up to 1.5 volts that largely exceeds the breakdown potential of the lipid bilayer, i.e. 150–500 mV.[38] It is reported that when an electric field is applied, voltage-sensitive protein channels open before the transmembrane potential reaches but voltages as large as KPFM reported results in direct membrane disruption.

All mentioned factors bother bacteria for several reasons: It is described[39] that the shape of the colonies of bacteria is markedly affected by the roughness of the surface and they prefer to stay on the valleys of the rough surfaces. The dimension of the roughness is also a determining factor in such a way that the density of bacteria on smooth surfaces is higher than in those samples having microroughness in the surface.[40] Consequently, the bacteria would prefer to stay on glass areas (smooth surfaces) than near the feldspar crystallizations (forming microroughness). Moreover, glass containing Calcium facilitates the adhesion of bacteria at low concentration but it could provoke the disruption of the cell wall for higher concentrations. Ca^{2+} is a glass stabilizer that up to a certain amount prevents the chemical degradation of the glass. The chemical composition of the glaze for ceramic tile has shown a low lixiviation rate accordingly with the expected durability of the tile surface. It has been reported[41] that the adhesion of bacteria to mucin (the main component of biofilm) involves a mechanism consisting of surface proteins in the bacteria that bind Ca^{2+}. So, the existence of a surface rich in calcium does not result in bacteria death, but in the opposite way, it helps their fixation on the surface of the glaze. In this sense, the low bactericide effect observed in both standard glazes is in agreement, with the fact that the glassy matrix is not deleterious by itself to the bacterial survival. The microroughness of such standard glazes seems to slightly limit bacterial growth. Conversely, the presence of regions with electrical charges at the feldspar crystallizations causes bacterial death (figure 6). The integrity and morphology of bacteria are sustained by the cell wall and the existence of electrical charges provokes the bacterial inactivation. The current dogma is that irreversible cell membrane electro-permeabilisation causes the death of the bacteria.[42]
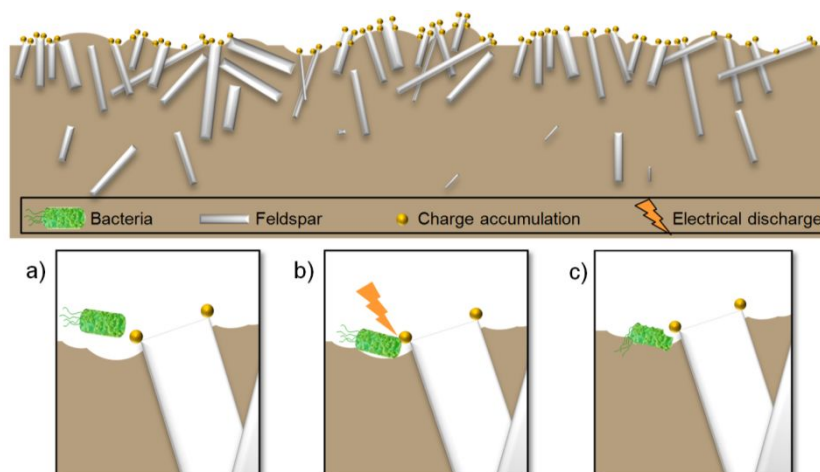
13

Figure 6.- Scheme of the combined glaze A+B after the sintering process and mechanism for bacteria death. a) Bacteria fixation at the glaze surface. b) Bacteria inactivation due to the electrical charge accumulation available at the glass-free feldspar crystallizations. c) Bacteria death.

The durability of the usual bactericide products based on chemical lixiviation is very limited. Most of them are organic compositions that are applied as external covers. In the case of inorganic materials as TiO_2, they should be previously irradiated with UV light in order to photoactivate the electron-hole separation and hence the bactericide effect is promoted. Bactericide effect in matrixes having Ag^+ decreases over time as the cations lixiviation rate decrease. In this work, the combination of glazes A and B allows the formation of platelet shape crystallizations that protrude from the surface and generate semiconductor-insulator interface barriers. The electrical charge accumulated at such interface barrier became an effective bactericide mechanism with R values >4 for both positive and negative gram bacteria. The proposed mechanism works without external light irradiation as occurs in photocatalyst mechanisms. Since the crystallizations are anchored to the glassy phase that forms part of the glaze, the durability of the effect endures over time up to the expected life of the glaze finishes. The long duration of the antibacterial effect is due to the presence of these crystallizations in the bulk of the glaze. Thus, an effective bactericide product for ceramic applications with extended durability has been obtained. The employed methodology opens new ways of research to achieve functional surfaces by the existence of crystallizations.

4.- Conclusions

A new glaze was designed through the combined layer deposition of standard glazes for the ceramic tile industry. The combination of two glaze compositions that are formulated with different Zn^{2+} content, which result in differences in evolution with temperature, such as melting

14

behaviour and crystallizations. The combined glaze promotes the appearance of protruding feldspar crystallization. The glass-free platelet crystallizations correspond to semiconductor feldspar in an insulator glass matrix. According to the KPFM analysis, the protrude crystallizations form Semiconductor-Insulator Interface barriers. The positive charge is accumulated at the interface barrier with potential values up to 1.5 volts that provokes the bacterial death. The electric potential present at the interface barriers exceeds largely the membrane breakdown potential of bacteria. Due to the inorganic nature of the feldspar crystallizations and their distribution in the whole glaze, the bactericide properties last for long periods of time. Thus, lasting antimicrobial surfaces for tiles have been obtained by using a different methodology of glaze deposition.

ACKNOWLEDGEMENTS

SUPPLEMENTARY INFORMATION

In this section, a escheme of the deposition of the glaze A and glaze B (both with different amount of ZnO in their composition) is shown in order to achieve feldspar crystallizations at the surface of glaze A+B (Figure S1). Glaze A+B presents higher antimicrobial activity than other glazes in bibliography and the antimicrobial activity is not related to the amount of ZnO of CaO in the composition (Figure S2). A RBS study demonstrates the homogeneous distribution of Zn at the whole glaze A+B layer (Figure S3). In addition, needle shape crystallizations of feldspar are distributed along with the glaze layer and outcrop from the surface (Figure S4). In the case of glaze A (glaze with ZnO), it presents feldspar crystallizations but they are not present at the surface (Figure S5). This difference with glaze A+B is responsible of the differences in antimicrobial activity.

References

[1] Savvova, O. V.; Bragina, L. L. Antibacterial Composite Glass Coatings for Protecting Special Purpose Steel Panels. *Glass and Ceramics*. **2010**, 67 (3-4), 123-125.

[2] Morelli, J. J.; Hogan, P. G.; Sullivan, M. L.; Muenks, C. E.; Wang, J. W.; Thompson, R. M.; Burnham, C-A. D.; Fritz, S. A. Antimicrobial Susceptibility Profiles of Staphylococcus aureus Isolates Recovered from Humans, Environmental Surfaces, and Companion Animals in Households of Children with Community-Onset Methicillin-Resistant S. Aureus Infections. *Antimicrobial Agents and Chemotherapy*. **2015**, 59 (10), 6634-6637.

15

[3] Flores, G. E.; Bates, S. T.; Caporaso, J. G.; Lauber, C. L.; Leff, J. W.; Knight, R.; Fierer, N. Diversity, Distribution and Sources of Bacteria in Residential Kitchens. *Environ. Microbiol*. **2013**, 15(2), 588–596.

[4] Delibas, M. T. Antibacterial Portland Cement. U.S. Patent 2014/0261074 A1, Sept, 2014.

[5] Sethi, D.; Sakthivel, R. ZnO/TiO$_2$ Composites for Photocatalytic Inactivation of Escherichia coli. *Journal of Photochemistry & Photobiology, B: Biology.* **2017***, 168,117–123.

[6] Bakali, J. Bactericidal Ceramic Enamel and Uses Thereof. Europe Patent 0921105B1, 9 June, 1999.

[7] Moya, J. S.; Esteban-Tejeda, L.; Pecharromán, C.; Mello-Castanho, S. R. H.; da Silva, A. C.; Malpartida, F. Glass-powders with a High Content of Calcium Oxide: a Step Toward a "Green" Universal Biocide. *Advanced Engineering Materials*. **2011**, 13 (6), B256-B260.

[8] Wen-Ru Li, Xiao-Bao Xie, Qing-Shan Shi, Shun-Shan Duan, You-Sheng Ouyang, Yi-Ben Chen, Antibacterial Effect of Silver Nanoparticles on Staphylococcus aureus. *Biometals*. **2011**, 24, 135–141.

[9] Cai, B.; Wang, P.; Yu, Z.; Zhang, X. Silver Ion Diffusion in Ion Diffusion Type Antimicrobial Ceramics. *Kuei Suan Jen Hsueh Pao/ Journal of the Chinese Ceramic Society.* **2005**, 33, 10, 1189-1192.

[10] Reinosa, J. J.; Romero, J. J.; Jaquotot, P.; Bengochea, M. A.; Fernandez, J. F. Copper Based Hydrophobic Ceramic Nanocoating. *Journal of the European Ceramic Society.* **2012**, 32(2), 277-282.

[11] Seabra, M. P.; Grave, L.; Oliveira, C.; Alves, A.; Correia, A.; Labrincha, J. A. Porcelain Stoneware Tiles with Antimicrobial Action. *Ceram. Int.* **2014**, 40, 6063–6070.

[12] Mettler, E.; Carpentier, B. Hygienic Quality of Floors in Relation to Surface Texture. *Trans IChemE*. **1999**, 77 (2), 90-96.

[13] Christine; A.; Roland. K.; Materials e.g. Polymer, Metal or Glass with Micro-roughened, Bacteria-repellent Surface. German Patent DE19818956A1, 26 november, 1998.

[14] Guoping Feng, Yifan Cheng, Shu-Yi Wang, Borca-Tasciuc, D. A.; Worobo, R. W.; Moraru, C. I. Bacterial attachment and biofilm formation on surfaces are reduced by small-diameter nanoscale pores: how small is small enough? *Biofilms and Microbiomes*. **2015**, 1, Article number: 15022.

[15] Lucas-Gil, E., Reinosa, J. J.; Neuhaus, K.; Vera-Londono, L.; Martín-González, M.; Fernández, J. F.; Rubio-Marcos, F. Exploring New Mechanisms for Effective Antimicrobial

16

Materials: Electric Contact-Killing Based on Multiple Schottky Barriers. *ACS Appl. Mater. Interfaces*. **2017**, 9 (31), 26219–26225.

[16] Reinosa, J. J.; Romero, J. J.; de la Rubia, M. A.; del Campo, A.; Fernández, J. F. Inorganic Hydrophobic Coatings: Surfaces Mimicking the Nature. *Ceram. Int*. **2013**, 39, 2489–2495.

[17] Polvorinos del Río, A.; Castaing, L.; Aucouturier, M. Metallic Nano-Particles in Lustre Glazed Ceramics From the 15th Century in Seville Studied by PIXE and RBS. *Nucl. Instr. Meth. B*. **2006**, 249 (1–2), 596–600.

[18] Helary, D.; Darque-Ceretti, E.; Aucouturier, M. Contemporary Golden-Like Lusters on Ceramics: Morphological, Chemical, and Structural Properties. *J. Am. Ceram. Soc*. **2005**, 88 (11), 3218–21.

[19] Leavitt, J. A.; Mcintyre, L. C.; Ashbaugh, M. D.; Oder, J. G.; Lin, Z. Cross Sections for 170.5° Backscattering of ^{4}He From Oxygen for ^{4}He Energies Between 1.8 and 5.0 MeV. *Nucl. Instr. Meth. B*, **1990**, 44 (3) 260–5.

[20] Mayer, M. SIMNRA User's Guide, Report IPP 9/113, Max-Planck-Institut für Plasmaphysik, Garching, Germany, 1997.

[21] Fortuna, D.; Martini, E. Antibacterial and Self-cleaning Ceramic Glazes. *Ceramic World Review*. **2010**, 89, 44-50.

[22] Chen, Z.; Mchale, J. M.; Antimicrobial Glaze and Porcelain Enamel Via Double Layer Glaze with High Zinc Content. European Patent EP1881892A4, 20 May, 2012.

[23] Özcana, S.; Acikbas, G.; Acikbas, N. C.; Induced Superhydrophobic and Antimicrobial Character of Zinc Metal Modified Ceramic Wall Tile Surfaces. *Applied Surface Science*. **2018**, 438, 136–146.

[24] Noguera, J. F.; Moreno, A.; Gozalbo, A.; Orts, M. J. Development of Ceramic Glaze Compositions with Bactericidal and Fungicidal Properties. Qualicer'10. **2010**, 1, 1-9.

[25] Hideki Yoshida, Hisao Abe, Toshitsugu Taguri, Fumihiko Ohashi, Shigeru Fujino, Toshihisa Kajiwara, "Antimicrobial Effect of Porcelain Glaze with Silver-clay Antimicrobial Agent. *Journal of the Ceramic Society of Japan*. **2010**, 118 (7), 571-574.

[26] Seabra, M. P.; Grave, L.; Oliveira, C.; Alves, A.; Correia, A.; Labrincha, J. A. Porcelain Stoneware Tiles with Antimicrobial Action. *Ceram. Int*. **2014**, 40, 6063–6070.
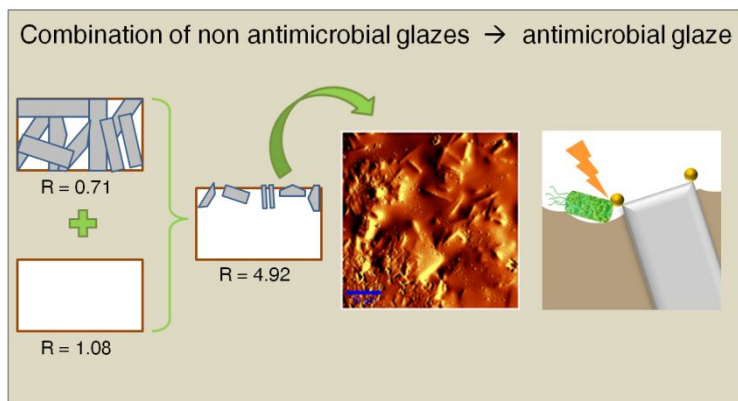
[27] Pekkan, K. The Thermal and Microstructural Behavior of a $R_2O–RO–(ZnO)–Al_2O_3–(TiO_2)–SiO_2$ Based Macro-crystalline Raw Glaze System. *Ceram. Int.* **2015**, 41, 7881–7889.

[28] Mestre, S.; Gómez, M. P.; Agut, P.; Barba, A.; Añó, E. Synthesis of Frits with ZnO Made From Zamak Waste. *CFI-Ceramic Forum international*. **2008**, 7, 15-25. 2008

[29] Fuertes, V.; del Campo, A.; Fernández, J. F.; Enríquez, E. Structural Insights of Hierarchically Engineered Feldspars by Confocal Raman Microscopy. *J. Raman Spectrosc.* **2019,** 50, 741–754.

[30] Epstein, W.; Schultz, S. G. Cation Transport in Escherichia coli. *The Journal of General Physiology.* **1965**, 49, 221-234.

[31] Tamayo, A.; Mazo, M. A.; Rubio, F.; Rubio, J. Application of the Raman and IR/ATR Spectroscopies to the Study of the Glasses upon Grinding. *Boletín de la Sociedad Española de Cerámica y Vidrio*. **2008**, 47 (2), 89-94.

[32] Avadhesh Kumar Yadav, Prabhakar Singh. A Review of the Structures of Oxide Glasses by Raman Spectroscopy. *RSC Adv.* **2015**, 5, 67583-67609.

[33] Freeman, J. J.; Wang, A.; Kuebler, K. E.; Jolliff, B. L.; Haskin, L. A. Characterization of Natural Feldspars by Raman Spectroscopy for Future Planetary Exploration. *The Canadian Mineralogist*. **2008**, 46,1477-1500.

[34] Parc, R.; Champagnon, B.; Dianoux, J.; Jarry, J.; Martinez, V. Anorthite and $CaAl_2Si_2O_8$ Glass: Low Frequency Raman Spectroscopy and Neutron Scattering. *Journal of Non-Crystalline Solids.* **2003**, 323, 155–161.

[35] Fuertes, V.; Cabrera, M. J.; Seores, J.; Muñoz, D.; Fernández, J. F.; Enríquez, E. Microstructural Study of Dielectric Breakdown in Glass-Ceramics Insulators. *Journal of the European Ceramic Society*. **2019**, 39, 376–383.

[36] Kerchove, A. J.; Elimelech, M. Relevance of Electrokinetic. Theory for "Soft" Particles to Bacterial Cells: Implications for Bacterial Adhesion. *Langmuir*. **2005**, 21, 6462-6472.

[37] Amit Kumar Prasad, Mayank Jain, Breakdown of Kasha's Rule in a Ubiquitous, Naturally Occurring, Wide Bandgap Aluminosilicate (Feldspar). *Scientific Reports*. **2018**, 8, 810.

[38] Unal, R.; Yousef, A. E.; Dunne, C. P. Spectrofluorimetric Assessment of Bacterial Cell Membrane Damage by Pulsed Electric Field. *Innov. Food Sci. Emerg. Technol*. **2002**, 3 (3), 247–254.

[39] Díaz, C.; Cortizo, M. C.; Schilardi, P. L.; Gómez de Saravia, S. G.; Fernández Lorenzo de Mele, M. L. Influence of the Nano-micro Structure of the Surface on Bacterial Adhesion. *Materials Research*. **2007**, 10 (1), 11-14.

[40] Karl Shellenbergerand, Brucee Logan, Effect of Molecular Scale Roughness of Glass Beads on Colloidal and Bacterial Deposition, Environ. Sci. Technol. 2002, 36, 184-189.

[41] Geesey, G. G.; Wigglesworth-Cooksey, B.; Cooksey, K. E. Influence of Calcium and Other Cations on Surface Adhesion of Bacteria and Diatoms: a Review. *Biofouling*. **2000**, 15(1-3), 195-200.

[42] Pillet, F.; Formosa-Dague, C; Baaziz, H.; Dague, E.; Rols, M-P. Cell Wall as a Target for Bacteria Inactivation by Pulsed Electric Fields. *Scientific Reports*. **2016**, 6:19778.

19

Combination of non antimicrobial glazes → antimicrobial glaze

R = 0.71

R = 1.08

R = 4.92

For Table of Contents Only

The combination of non antimicrobian glazes, with different fluxing properties, in a determinated way gives raise to an antimicrobial glaze. The properties are due to the existence of feldspar crystallizations outcropping the surface and free of glassy phase, whose edges and corners present electrical charges which are able to denaturalized the external wall of microorganisms.

20